Fabian Steinmetz, Jan Heitmann, and Christian Renner. A Practical Guide to Chirp Spread Spectrum for Acoustic Underwater Communication in Shallow Waters. In Proceedings of the 13th ACM International Conference on Underwater Networks & Systems, WUWNet '18, Shenzhen, China, December 2018. **Best Paper Award**.

A Practical Guide to Chirp Spread Spectrum for Acoustic Underwater Communication in Shallow Waters

Fabian Steinmetz
Hamburg University of Technology
fabian.steinmetz@tuhh.de

Jan Heitmann
Hamburg University of Technology
jheitmann@tuhh.de

Christian Renner
Hamburg University of Technology
christian.renner@tuhh.de

ABSTRACT

Small and cheap micro AUVs enable diverse underwater monitoring applications in shallow inshore waters; e.g., inspection of underwater assets, observation of water quality, and identification of pollution sources. The formation and collaboration of swarm members yet requires communication and self-localization based on cheap, miniature acoustic devices. However, this is severely hampered by the effects of multi-path propagation and scattering in shallow waters. In general, we discovered improvements of chirp-based—i.e., frequency-sweep—synchronization in these scenarios. This paper presents strategies to find proper chirp parameters. First, we study the benefits and applicability of chirp-based modulation against FSK. Second, we discuss the impact of the chirp parameters in real-world scenarios and identify sweep spots w.r.t. bandwidth to improve the standard deviation of the position in the time domain up to 86 % above this point. Third, we present instructions to choose these parameters in an efficient and appropriate way for any shallow water scenario.

1 INTRODUCTION

Exploration and monitoring of underwater sceneries is drawing considerable attention [11]. Recent examples are ship tracking in harbors [25], HydroNode [23], SUNRISE [30] or underwater services such as RoboVaaS [22].

Fine-grained measurements require a dense network of stationary sensors [20], mobile devices [10, 14], or both. Timely acquisition of data mandates communication - typically wireless to keep installation and maintenance cost low or allow the integration in μAUVs with a wide operation range. Due to the strong damping of the electro-magnetic wave in the water, most of the communication interfaces use an acoustic communication. Acoustic underwater modems have been proposed by academia [2, 7, 9, 27] and launched by industry [4, 8, 32] for this purpose. Shallow and relatively small water bodies—such as port basins, lakes, or canals—are a particularly challenging scenery; models have been derived for theoretic analysis and simulation [3, 31]. In addition to distance- and frequency-related signal fading as described in [29], the shallowness and obstacles—e.g., walls and plants—further hamper reliable communication and localization [13, 26]. Reflections and scattering at the water surface cause massive inter- and intra-symbol interference, because the non-line-of-sight (NLOS) signals have a low delay and attenuation only [15].

Moreover, obstacles are additional sources of signal reflections while they may also prevent line-of-sight (LOS) communication. In previous research [27] and recent measurement campaigns, we experienced significant attenuation and amplification of frequency shares depending on position and time. In [12] we presented a narrow-band chirp-based preamble synchronization and compared the results to a frequency shift keying (FSK)-based preamble synchronization. The chirp-based synchronization was motivated by the following observations. Failure detection arises mainly from cancellation and amplification caused by reflections and scattering. The main reason for this is intra-symbol interference leading to unreliable symbol detection and hence synchronization. Once the synchronization has succeeded, however, the symbol windows are known and communication can be achieved through relatively simple methods such as frequency hopping and redundancy coding. Due to their excellent correlation properties, chirps are widely used in radar applications. Likewise, chirps are already employed for data transmission. In the year 1992 a patent [34] was received for a chirp-based data transmission over power distribution lines. Other recent examples are LoRa [28], aerial acoustic communication [18] and already underwater acoustic communication [6, 17, 19]. The authors in [16] give additional a theoretical introduction about choosing parameters for a chirp-based data transmission and evaluate these parameters in a real world scenario. The mentioned chirp-based underwater communication use, compared to our underwater modem, huge and powerful devices. Our future purpose is to use chirp modulation with a low-power, low computational capacity and small underwater modem.

The discussed narrow-band chirp-based synchronization [12] enhances the detection probability, accuracy and precision in comparison to the FSK synchronization. Chirp signals spread the information over a frequency band and provide brighter correlation properties in comparison to the FSK symbols. Now, we want to improve the chirp-based synchronization and study the effect of wider bandwidths. To improve the chirp-based synchronization and transmission, we decided to compare different chirp symbols in different scenarios in a detailed real-world evaluation.

1.1 Contributions

We motivate the benefit of chirp symbols against symbols with a constant frequency, for example FSK symbols. We sketch a detection method for both symbol types and explain the influence of symbol parameters; e.g. carrier-frequency, symbol length and bandwidth. We evaluate our detection method and different parameter settings

WUWNet'18, December 3–5, 2018, Shenzhen, China

ACM ISBN 978-1-4503-6193-4/18/12…$15.00
https://doi.org/10.1145/3291940.3291964

in a real-world environment with shallow-water conditions. We conclude with instructions to design a chirp-based communication in a shallow-water scenario.

Our results are based on real-world experiments in conditions similar to typical inshore, shallow-water application scenarios. Due to the generality of our findings, the results can be exploited to elevate recent attempts to standardize digital underwater communication such as JANUS [24].

2 FUNDAMENTALS

The following section gives a brief discussion on the signals and data modulation. Furthermore, detection methods are introduced and compared.

2.1 Frequency-Shift Keying

Frequency-Shift Keying (FSK) is commonly used in acoustic underwater communication [2, 4, 9], e.g., as part of JANUS [24]. In binary frequency-shift keying (BFSK), a bit b is transmitted as a sinusoidal symbol with frequency f_b, duration T and a carrier frequency f_0. There are more complex forms of FSK, which we do not address in detail due to space constraints. The transmitted symbol $s(t)$ centered at $t = 0$ describes

$$s(t) = \begin{cases} \sin\left(2\pi\left(f_0 + f_b\right)t\right) & \text{if } |t| < T/2, \\ 0 & \text{otherwise.} \end{cases} \tag{1}$$

2.2 Chirp Keying

A linear chirp symbol $s(t)$ centered at $t = 0$ describes

$$s(t) = \begin{cases} \cos\left(2\pi f_0 + \pi\mu t^2 + \phi_0\right) & \text{if } |t| < T/2, \\ 0 & \text{otherwise} \end{cases} \tag{2}$$

with the carrier or center frequency f_0, chirp rate μ, phase ϕ_0 [5]. The chirp bandwidth B is defined by

$$B = |\mu|\, T. \tag{3}$$

In the following a chirp with positive chirp rate is called an up-chirp and with a negative chirp rate a down-chirp. A simple chirp keying modulates a bit b to the chirp rate. For example

$$\mu_b > 0 \Rightarrow \text{up-chirp} \qquad \text{if } b = 0, \tag{4}$$

$$\mu_b < 0 \Rightarrow \text{down-chirp} \qquad \text{if } b = 1. \tag{5}$$

2.3 Symbol Detection

There exists a plethora of different detection methods to design a receiver structure. For instance, the non-coherent detection implemented in our modem firmware for an FSK transmission. In relation to chirp-modulation [1] uses the non-coherent detection to receive transmitted chirps. The non-coherent receiver measures the similarity between a received signal and a stored reference signal. This leads to the requirement of a previous synchronization between transmitter and receiver.

A matched filter or correspondingly the cross-correlation measures the similarity and additionally the time delay. In general, we decide between two detection purposes: (1) Synchronization: The receiver does not know the timings (symbol frames) of the received sequence. In order to perform a correct data detection and demodulation, the receiver has to synchronize to the received sequence.

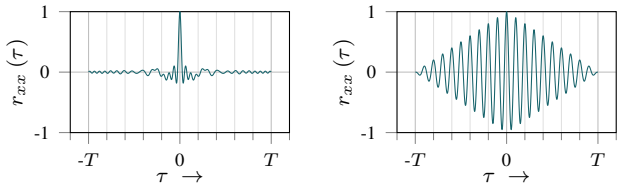

(a) Chirp symbol (b) FSK symbol

Figure 1: Auto-correlations $r_{xx}(\tau)$ functions (normalized to 1) of chirp and FSK symbols.

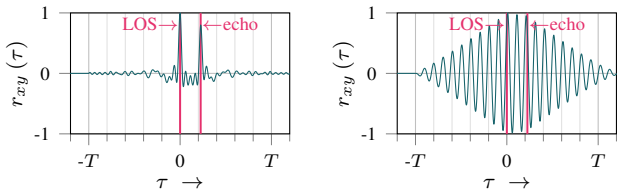

(a) Chirp symbol (b) FSK symbol

Figure 2: The LOS path (arrives at $t = 0$) is superimposed with a damped (damping factor 0.8) and delayed (arrives at $\tau = 0.225T$) signal from a NLOS path (echo). The plots show the cross-correlations (normalized to 1) between the received signal and the reference symbol.

(2) Data demodulation: The receiver is synchronized with the received sequence and knows the symbol frames. In this case the receiver splits the received sequence into symbols and demodulates each symbol.

This paper focuses on the synchronization with a received sequence, respectively symbol, using a matched filter. In previous research we presented a small, low-power and low-cost acoustic underwater modem [27]. Against the background of our system requirements, we use a packet-based transmission with a preamble-based synchronization. We discovered that an accurate synchronization leads to a more reliable data reception with our underwater modem [12], so we want to improve the accuracy and precision of the synchronization. A second reason, which requires an accurate synchronization are distance measurements and self-localization [13]. Using a time-of-flight estimation between two underwater modems, their distance can be determined. With the knowledge of the position of different reference nodes (other underwater modems) and distance measurements, a μAUV can localize itself.

3 MATCHED FILTER RECEIVER

A matched filter measures the displacement in time domain and the similarity between a received symbol $r(t)$ and a stored symbol $s(t)$. The displacement in the time domain can be used to synchronize the receiver. Matched filters are widely employed in radar- and communication systems. Further information and a more theoretical background are given for example in [33].

A matched filter is the optimum receive filter in the case of an additive white Gaussian noise channel, which maximizes the signal-to-noise ratio at the filter output. The matched filter filters the received signal with the inverse transmission filter. This operation equals a cross-correlation with the transmission filter. In relation to different transmitted symbols (here up- and down-chirps), the

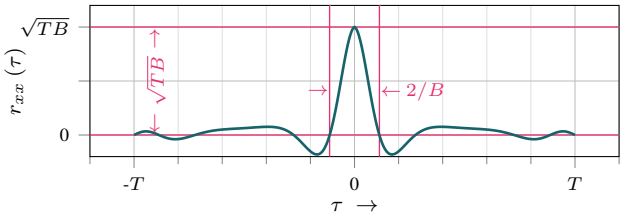

Figure 3: Chirp auto-correlation function properties. This figure depicts the envelope (Eq. (8) with $f_0 = 0$) of the auto-correlation function.

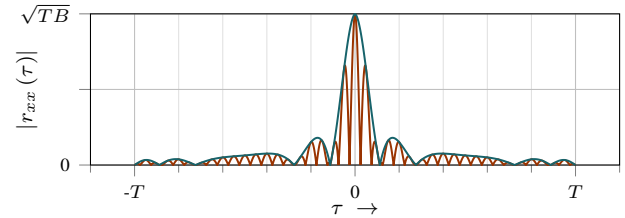

Figure 4: Absolute envelope ($f_0 = 0$) of the chirp auto-correlation function in blue and absolute chirp auto-correlation function of a chirp with $f_0 = B$ in red.

cross-correlation is calculated between the transmitted and received symbol.

The cross-correlation $r_{xy}(\tau)$ between the signals $x(t)$ and $y(t)$ is defined by

$$r_{xy}(\tau) = \int_{-\infty}^{\infty} x^*(t) \cdot y(t+\tau) \mathrm{d}t \tag{6}$$

with the conjugate complex signal $x^*(t)$ of $x(t)$. The displacement τ_{delay} between $x(t)$ and $y(t)$ (a time-shifted version of $x(t)$) is

$$\tau_{\text{delay}} = \arg\max_{\tau}(r_{xy}(\tau)). \tag{7}$$

Figure 1 depicts the cross-correlations between two chirp symbols and two FSK symbols, without a time-shift ($y(t) = x(t)$). This special case is defined as auto-correlation $r_{xx}(\tau)$. The chirp auto-correlation function output is a small thin peak with narrow sidelobes. Opposed to that, the envelope of the FSK symbol auto-correlation function has triangular shape.

Furthermore, in underwater communication scenarios the acoustic wave is reflected and scattered at other objects, e. g. the water surface. In Fig. 2 the LOS signal is interfered with a NLOS signal (echo) from the water surface. The arrival delay of the NLOS signal is $0.225T$ and the damping 0.8 (in this example). This results in a second peak in the cross-correlation between the received and stored reference signal. The peaks in the chirp cross-correlation function have a clear separation between each other. On the contrary, the FSK cross-correlation superimposes the single shapes and a distinction between the peaks is more difficult or almost impossible.

In order to analyze the chirp auto-correlation function $r_{xx}(\tau)$, it can be written as (cf. [5]):

$$r_{xx}(\tau) = \sqrt{BT} \frac{\sin\left(\pi B\tau\left(1 - \frac{|\tau|}{T}\right)\right)}{\pi B\tau} \cos(2\pi f_0 \tau). \tag{8}$$

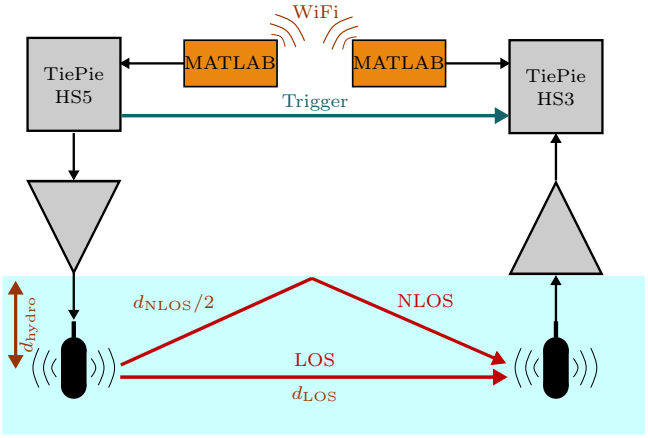

Figure 5: The upper part illustrates the hardware structure, used in the real-world evaluation. Signal generation and recording is done with two TiePie USB oscilloscopes and MATLAB. The signals were fed to our receive and transmission circuits, which are connected to two transducers. Furthermore, at the lower part of the figure, LOS and NLOS are depicted.

Based on that, the first zeros of the envelope (Eq. (8) with $f_0 = 0$) are located at $|\tau| \approx 1/B$. The peak is $\sqrt{BT}$ high. A graphical interpretation gives Fig. 3.

Carrier frequencies $f_0 > B/4$ (if the first envelope zeros locate at $|\tau| = 1/B$) produce additional zeros closer to the origin, but the shape remains the same. The absolute envelope ($f_0 = 0$) of the chirp auto-correlation function and an other absolute chirp auto-correlation function of a chirp with $f_0 = B$ depicts Fig. 4 as an example.

4 EXPERIMENTATION SETUP

Figure 5 depicts the used hardware structure. In general, we use two TiePie USB oscilloscopes and aribitrary waveform generators[1], each connected to a Laptop with MATLAB. The TiePie HS5 on the transmitter side receives the generated signal from MATLAB. The output of the waveform generator is connected to the transmission circuitry of our smartPORT acoustic modem [27], a low-power, low-cost device for use in μAUVs such as Hippocampus [10]. When the signal transmission starts, the generator uses a trigger to start the signal recording at the receiver side. The trigger signal is directly connected through a shielded twisted-pair cable. Signal recording is done with a TiePie HS3 at the receiver circuit of our modem. In order to use a wide frequency range, the analogue band-pass filter is bridged. The WiFi connection between the laptops with MATLAB establishes a coordination through large measurement sessions.

In all cases the sampling rate was 1 MHz and the synchronization ground-truth was obtained with 50 long, wide-band up-chirps (0 kHz to 100 kHz, 10 ms). We use an Aquarian Audio AS-1[2] hydrophone as transducer. We use our modem circuits without the bandpass filter, but additional the hydrophones have a frequency-dependent behavior, shown in Fig. 6. All tests are executed with a carrier frequency in the range from 10 kHz to 100 kHz. In this

[1] https://www.tiepie.com/en/usb-oscilloscope
[2] http://www.aquarianaudio.com/as-1-hydrophone.html

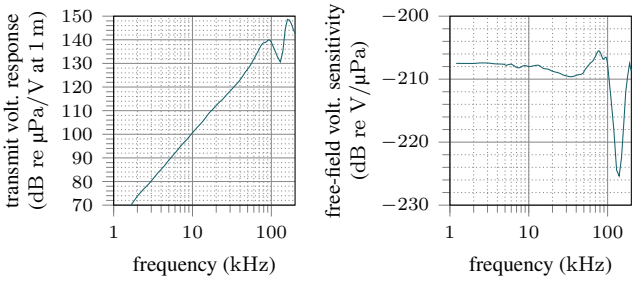

(a) AS-1 as transmitter (b) AS-1 as receiver

Figure 6: Hydrophone characteristics as a receiver or transmitter. The characteristics are explained in [27].

range the frequency dependent behavior varies up to 40 dB. In our evaluation we compare the results without any additional filter to a setup with a filter, which enhances the lower part up to 20 dB before the transmission. Here we try to compensate the frequency behavior, in order to distribute the transmitted power more consistent over the frequencies. Unless stated otherwise, the results are measured without the transmission filter.

Additionally to the effect of the hydrophone characteristics, the transmission loss due to friction varies between ~ 1 dB/km and ~30 dB/km (for frequencies between 10 kHz and 100 kHz)[21]. In our scenarios we transmit over several meters, means the frequency dependent transmission loss can be neglected compared to the effect of the hydrophone characteristic.

The hydrophones were placed in a shallow water scenario with a line-of-sight (LOS) and non-line-of-sight (NLOS) signal propagation path. One major aspect in this scenario is the reflection at the water surface, here the strongest NLOS propagation path [12]. In this scenario the path length d_{NLOS} can be calculated with the Pythagorean theorem

$$d_{\text{NLOS}} = 2 \cdot \sqrt{\left(\frac{d_{\text{LOS}}}{2}\right)^2 + d_{\text{hydro}}^2} \tag{9}$$

with the LOS path length d_{LOS} and the depths of the hydrophones under the water surface d_{hydro}. This results in a time difference of the arrival time between LOS and NLOS

$$\Delta t_{\text{TOA}} = \frac{d_{\text{NLOS}} - d_{\text{LOS}}}{v_{\text{sos}}} \tag{10}$$

with the speed of sound v_{sos}.

For evaluation of different FSK and chirp symbols, we conducted tests in three different scenarios (see Table 1). First, we perform a small-scale test in a tank in our laboratory (Fig. 7). The LOS distance was 56 cm, the water depth 20 cm, the tank width 40 cm and the hydrophones were placed at a depth of 7.5 cm. In order to avoid strong reflections from the areas behind the hydrophones, eggbox foam was mounted. However, this scenario provides reflections at the walls and the ground in addition to the surface reflection. This scenario could take place in a corner of a quay wall or a pipe system.

The other evaluations took place at the Harburger Hafen, a small marina in Hamburg. Here, the hydrophones had LOS distances of 6.12 m and 13.8 m (Fig. 8a), depth of 1.1 m and the supports were mounted on a jettie (Fig. 8b). The water was at least 2.5 m deep,

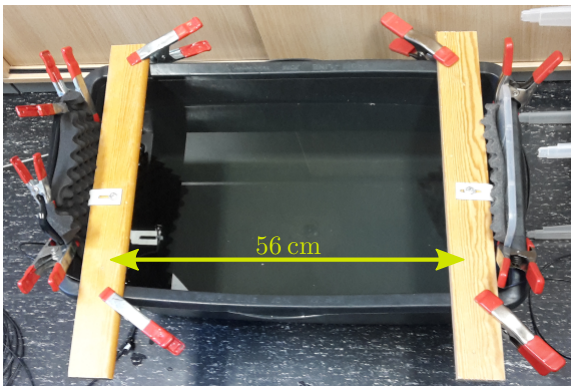

Figure 7: Laboratory small-scale test in a tank. The hydrophones were mounted with a distance of 56 cm and at a deep of 7.5 cm. In order to avoid too much reflections behind the hydrophones eggbox foam was mounted.

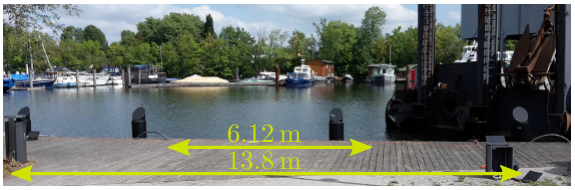

(a) Transmission distances d_{LOS}. The hydrophones were mounted with a distance of approximately 1.7 m to the jettie and at a depth of 1.1 m.

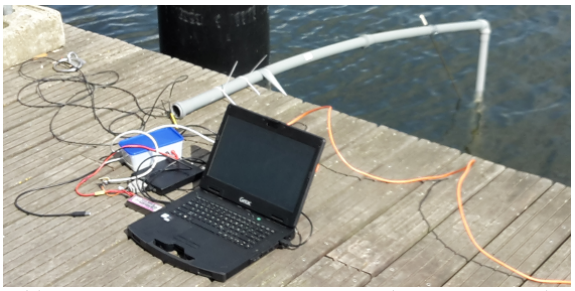

(b) Hydrophone support and receiving part (right side in Fig. 5)

Figure 8: Test settings of our real-world evaluation at the marina in Hamburg.

Table 1: Evaluation scenarios in our real-world study. The length of the propagation path, which is reflected at the water surface d_{NLOS} is calculated with the help of Eq. (9). Additional the speed of sound is assumed as $v_{\text{sos}} = 1480\,\text{m}\,\text{s}^{-1}$.

	Laboratory	Harbour Test 1	Harbour Test 2
d_{LOS}	0.56 m	6.12 m	13.80 m
d_{hydro}	0.075 m	1.1 m	1.1 m
d_{NLOS}	0.58 m	6.50 m	13.97 m
t_{LOS}	0.38 ms	4.14 ms	9.32 ms
Δt_{TOA}	13 µs	259 µs	118 µs

had a salinity of 0.237 ppt and the temperature was 22 °C (6.12 m evaluation) respectively 19 °C (13.8 m evaluation). Based on [21], the speed of sound is 1488 m s^{-1} and 1479 m s^{-1}. These scenarios could be a near field communication for example between sensor nodes or μAUVs in a swarm.

5 EVALUATION AND RESULTS

We evaluate the impact of the bandwidth, the symbol length, the hydrophone characteristic and the detection algorithm. At the beginning of this section we compare single measurements with variations in these parameters, followed by large-scale evaluations with thousands of measurements. The current FSK implementation of our underwater modem uses a symbol length of 2.5 ms (500 samples with 200 kHz sampling rate) [27]. During the evaluation we chose smaller and longer symbol lengths.

5.1 Bandwidth

First, we evaluate the impact of the chirp bandwidth B. A larger bandwidth gives a shorter peak, and the time distance between the first zero is approximately $2/B$ (cf. Sect. 3). Based on that, the required bandwidth to have a complete separation between the LOS and NLOS signal from the water surface is $B = 2/\Delta t_{\text{TOA}}$ (the right LOS peak zero in Fig. 3 is at the same position with the left NLOS peak zero). The bandwidth is usually limited in communication systems. The limitation depends on the transmitter and receiver type and interference with other communication systems in the same frequency region or regulations.

Figures 9 and 10 depict the results of cross-correlations in the laboratory and the second harbour evaluation. Using the results in Table 1 these bandwidths are $B_{\text{lab}} = 2/13\,\mu\text{s} = 153.8\,\text{kHz}$ and $B_{\text{har2}} = 2/118\,\mu\text{s} = 16.9\,\text{kHz}$. Of course, it is not necessary to have completely separated peaks, but these values give a good classification. Both figures show the cross-correlations with the symbol bandwidths $B \in \{0\,\text{kHz}, 5\,\text{kHz}, 10\,\text{kHz}, 50\,\text{kHz}\}$ and $f_0 = 70\,\text{kHz}$ (all frequencies are in the upper linear part of the hydrophone characteristic), $T = 1\,\text{ms}$. The case $B = 0\,\text{kHz}$ corresponds to a FSK symbol.

In all cases, in Fig. 9 a clear separation between the different peaks and detection of the first peak is not possible. The reflection from the walls and the bottom in the small tank adds a large amount of propagation paths, resulting in many peaks in the cross-correlations. Opposed to that, up- and down-chirps with bandwidths $B \in \{5\,\text{kHz}, 10\,\text{kHz}, 50\,\text{kHz}\}$ at distance $d_{\text{LOS}} = 13.8\,\text{m}$ (cf. Fig. 10) give a clear separation in the cross-correlation. In addition, a shorter peak establishes a more precise detection of maximum peak position. In summary, the results confirm the theoretical background in Sect. 3. A higher bandwidth leads to a shorter peak in the cross-correlation function.

5.2 Symbol Length

During the second real-world test, we evaluated different symbol lengths $T \in \{1\,\text{ms}, 2.5\,\text{ms}, 5\,\text{ms}, 10\,\text{ms}\}$ and fixed other parameters $B = 20\,\text{kHz}$, $f_0 = 70\,\text{kHz}$ in two different scenarios. The data rate is directly linked to the symbol length (when the bits per symbol remain constant). A smaller symbol length yields a faster data rate.

The first experiment in the laboratory and the second evaluation were done in the larger harbour test. The cross-correlation peak high is scaled with $\sqrt{BT}$ (see Sect. 3). However, the peaks from the NLOS paths are also enhancing with a longer symbol length. In all cases the arrival time of the reflections are much smaller than the symbol length, resulting in intra-symbol interference.

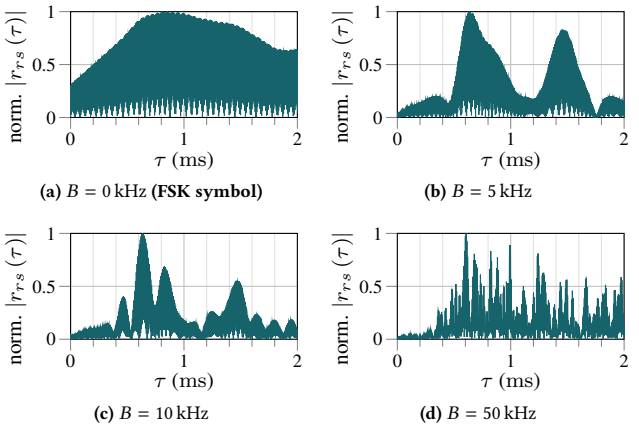

(a) $B = 0\,\text{kHz}$ **(FSK symbol)** **(b)** $B = 5\,\text{kHz}$

(c) $B = 10\,\text{kHz}$ **(d)** $B = 50\,\text{kHz}$

Figure 9: Laboratory ($d_{\text{LOS}} = 0.56\,\text{m}$, $t_{\text{LOS}} = 0.38\,\text{ms}$): cross-correlations (normalized to 1) between a received chirp and the stored reference chirp. In all cases up-chirps with $T = 1\,\text{ms}$, $f_0 = 70\,\text{kHz}$ are used and a variation in B. The time difference between the LOS and the surface reflection (NLOS) is $\Delta t_{\text{TOA}} = 13\,\mu\text{s}$.

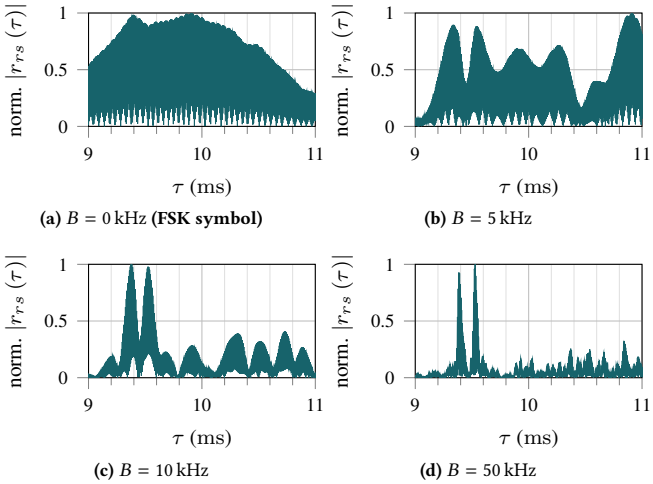

(a) $B = 0\,\text{kHz}$ **(FSK symbol)** **(b)** $B = 5\,\text{kHz}$

(c) $B = 10\,\text{kHz}$ **(d)** $B = 50\,\text{kHz}$

Figure 10: Harbour test 2 ($d_{\text{LOS}} = 13.8\,\text{m}$, $t_{\text{LOS}} = 9.32\,\text{ms}$): cross-correlations (normalized to 1) between a received chirp and the stored reference chirp. In all cases up-chirps with $T = 1\,\text{ms}$, $f_0 = 70\,\text{kHz}$ are used and a variation in B. The time difference between the LOS and the surface reflection (NLOS) is $\Delta t_{\text{TOA}} = 118\,\mu\text{s}$.

In conclusion, the cross-correlations in Fig. 11 and Fig. 12 equal for all symbol lengths. In rare situations we detected improvements at lower carrier frequencies with a higher damping (compare to Fig. 6) with a longer symbol length.

5.3 Peak Detection

When the cross-correlation was calculated (cf. Sect. 3), the purpose is to find the peak from the LOS signal to improve an exact synchronization to the received signal.

The elementary approach is to find the maximum value of the whole absolute cross-correlation. A disadvantage could be, that a higher peak of a (delayed) NLOS signal (for example in Figs. 12a, 12b and 12d) leads to a false synchronization.

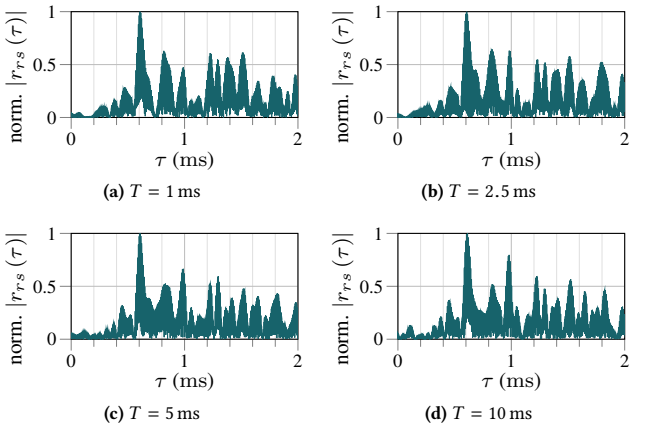

(a) $T = 1$ ms (b) $T = 2.5$ ms (c) $T = 5$ ms (d) $T = 10$ ms

Figure 11: Laboratory: cross-correlations (normalized to 1) between a received chirp and the stored reference chirp. In all cases up-chirps with $f_0 = 70$ kHz, $B = 20$ kHz are used and a variation in T.

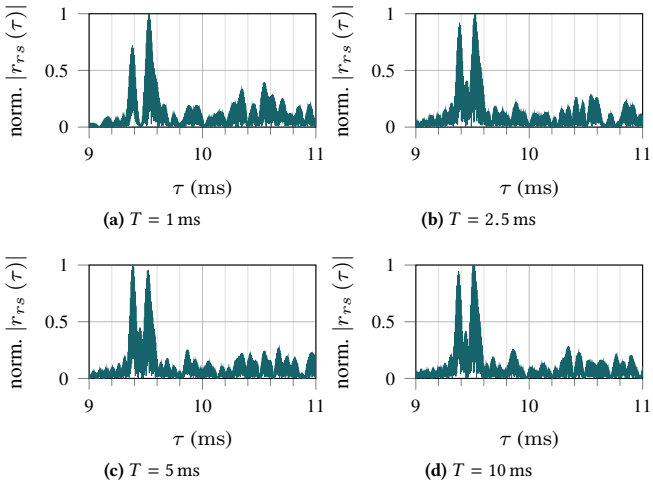

(a) $T = 1$ ms (b) $T = 2.5$ ms (c) $T = 5$ ms (d) $T = 10$ ms

Figure 12: Harbour test 2: cross-correlations (normalized to 1) between a received chirp and the stored reference chirp. In all cases up-chirps with $f_0 = 70$ kHz, $B = 20$ kHz are used and a variation in T.

We developed a different algorithm to find the first peak: (1) Find local maxima over a threshold γ_{dec}. (2) Choose the tallest maxima with a minimum distance $1/B$ to other selected maxima. (3) Use the first maximum as the LOS peak.

Currently, the detection threshold is related to the maximum of the cross-correlation $r_{sr}(\tau)$ between the received and transmitted symbol. The threshold is $\gamma_{\text{dec}} = 0.5 \cdot \max |r_{sr}(\tau)|$ and based on many real-world evaluations. In the future, we intend to change this to an adaptive threshold in relation to the signal and noise level and their correlation properties.

Figure 13 contains heatmaps with the distribution of the synchronization error compared to different frequencies. The synchronization error was calculated with the discussed ground-truth in Sect. 4. We choose carrier frequencies in the range from 20 kHz to 100 kHz with 5 kHz steps. Each carrier frequency we transmit 50 up-chirps and 50 down-chirps with different bandwidths ($B = 0$ kHz in Fig. 13a and $B = 30$ kHz in Figs. 13b and 13c) and a fixed symbol length $T = 1$ ms.

First, we show the high variance of synchronization position for symbols with a constant frequency ($B = 0$ kHz) detected with the maximum peak detection in Fig. 13a. A higher bandwidth reduces the variations in time domain, but the synchronizations are located at two regions. The first region has a mean of value -5.7 µs (57.6 % of the synchronizations are in the range -50 µs to 50 µs) and the second a mean of 138.9 µs (41.0 % of the synchronizations are in the range 100 µs to 150 µs), which is the time distance between the LOS path and the NLOS path reflected at the water surface $\Delta t_{\text{TOA}} = 118$ µs in Table 1. The values in Table 1 are measured with a measuring tape at the beginning of the evaluation, which explains the small differences.

Our second detection implementation (in Fig. 13c) solves the problem of synchronization to NLOS peaks. This yields a mean value of -7.4 µs in the region -50 µs to 50 µs, where 95.7 % of synchronizations are located. According to the results, our second implementation enhances the likelihood to find the right peak.

In the following evaluations we use the second implementation, which detects the first peak. It exists one exception for $B = 0$ kHz, because the minimum peak distance is usually set to $1/B$. In this case the minimum distance is set to the symbol length T.

5.4 Hydrophone Characteristic

Our hydrophones have a frequency-dependent behavior (cf. Fig. 6). A transmitted signal at 10 kHz has a 40 dB higher damping compared to a signal at 100 kHz. In the case of chirps with a wide bandwidth, the frequency components are transmitted with different amplitude (and power). Related to the characteristic, an up-chirp has a rising amplitude and a down-chirp a falling amplitude. For this reason we evaluate a rudimental compensation and apply a digital low-pass filter, which amplifies the lower frequencies up to 20 dB. We decided to use a smaller compensation in order to approach the filter cautiously. The evaluation takes place in the laboratory and the second harbour test. In both cases we transmitted chirps with different bandwidths $B \in \{10\,\text{kHz}, 20\,\text{kHz}, 30\,\text{kHz}, 50\,\text{kHz}\}$, symbol lengths $T \in \{1\,\text{ms}, 2.5\,\text{ms}\}$ at different carrier frequencies $f_0 \in \{50\,\text{kHz}, 55\,\text{kHz}, \ldots, 100\,\text{kHz}\}$. Each setup we transmitted 100 chirps and compare the standard deviation over all carrier frequencies (in the sum 1100 transmission). In all cases the standard deviation is slightly smaller without our compensation filter. Table 2 lists the results of our evaluation in the harbour. The reason can be explained as followed. In all transmissions the amplification factor of our transmitter remains the same and the filter increase the power density at frequencies with a higher damping. Furthermore, we transmitted 100 ms band-limited pseudo-random noise in the range 10 kHz to 50 kHz without and with filter. The power ratio of transmitted and received signal is 2.96 dB without filter and -2.42 dB with filter (the ratio is calculated between the generator output and the oscilloscope with the same amplification gains).

Based on the results, we decided to omit the compensation filter in the following, because the compensation leads to higher variance and a smaller ration between the received and transmitted signal.

5.5 Large-scale Evaluation

To prove our findings in Sects. 5.1 and 5.2, we performed a large-scale evaluation. With different bandwidths and symbol lengths we

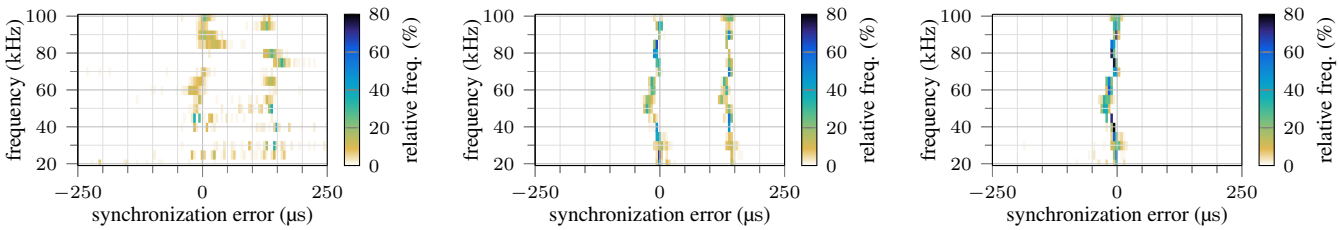

(a) B = 0 kHz, **max. peak detection** (b) B = 30 kHz, **max. peak detection** (c) B = 30 kHz, **first peak detection**

Figure 13: Heatmaps of synchronization errors for chirp detection with different detection algorithms and different bandwidths. The synchronization error has a time resolution of 5 µs **and was measured at a distance of** 13.8 m (Δt_{TOA} = 118 µs) **during the harbour evaluations.**

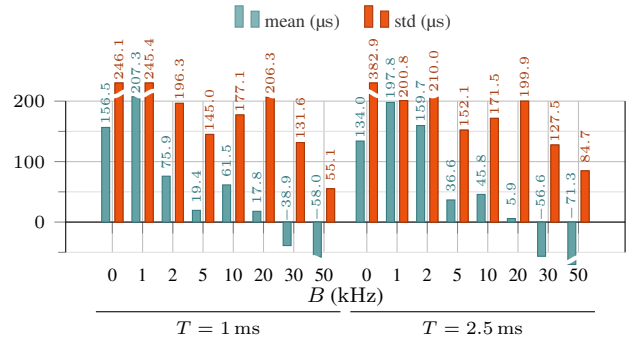

(a) Laboratory (d_{LOS} = 0.56 m, $2/\Delta t_{\text{TOA}}$ = 153.8 kHz)

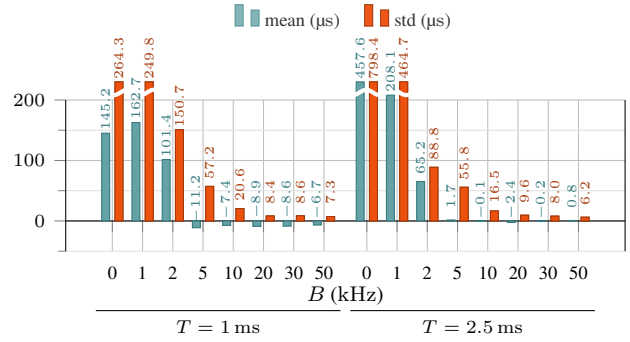

(b) Harbour Test 2 (d_{LOS} = 13.80 m, $2/\Delta t_{\text{TOA}}$ = 16.9 kHz)

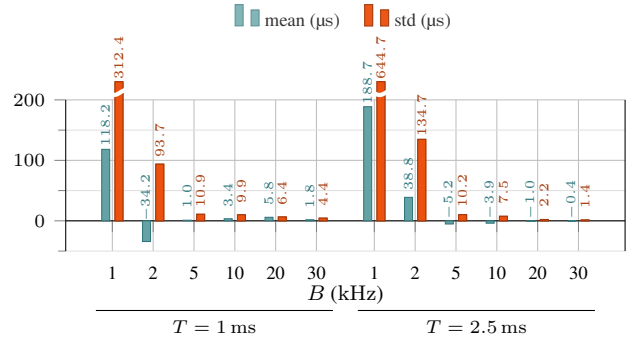

(c) Harbour Test 1 (d_{LOS} = 6.12 m, $2/\Delta t_{\text{TOA}}$ = 7.7 kHz)

Figure 14: Mean and standard deviation in relation to to the estimated time-of-flight (cf. Sect. 4). For different B and T we performed tests at $f_0 \in \{50\,\text{kHz}, 55\,\text{kHz}, \ldots, 100\,\text{kHz}\}$. Each f_0 we transmitted 50 **up- and** 50 **down-chirps. This results in** 1100 **transmissions per bar. Figures 14a and 14b use the same B setups compared to Fig. 14c.**

Table 2: Standard deviation of received chirps during with harbour test 2 (d_{LOS} = 13.8 m) without and including a compensation filter before transmitting the chirps.

B, T	1 ms	1 ms, **filter**	2.5 ms	2.5 ms, **filter**
10 kHz	12.2 µs	20.6 µs	15.0 µs	16.5 µs
20 kHz	8.7 µs	8.4 µs	8.8 µs	9.6 µs
30 kHz	8.7 µs	8.8 µs	8.1 µs	8.0 µs
50 kHz	6.9 µs	7.3 µs	5.4 µs	6.2 µs

performed tests in the laboratory and harbour at different carrier frequencies $f_0 \in \{50\,\text{kHz}, 55\,\text{kHz}, \ldots, 100\,\text{kHz}\}$. We transmitted 50 up-chirps and 50 down-chirps each carrier frequency. This results in 1100 transmissions. Figures 14a to 14c contain the mean and standard deviation in relation to the estimated time-of-flight (cf. Sect. 4).

Figure 14a shows high standard deviations for all bandwidths, resulting from the massive reflections inside the small tank in the laboratory. However, an increasing bandwidth decrease the standard deviation. Surprisingly, the results for lower bandwidths (0 kHz − 2 kHz) and B = 1 ms in the laboratory resemble the values in Fig. 14b.

Furthermore, the evaluation in the harbour (Figs. 14b and 14c) points out that there exists a sweep spot w.r.t. bandwidth. Behind this point the standard deviation of the position rapidly decreases. In Fig. 14b a complete peak separation (LOS and NLOS) requires $2/\Delta t_{\text{TOA}}$ = 16.9 kHz bandwidth. Increasing the bandwidth from 2 kHz to 5 kHz improves the standard deviation up to 62 % (T = 1 ms), from 2 kHz to 10 kHz up to 86 %. The following step to B = 10 kHz has a 95 % improvement compared to B = 2 kHz. Higher bandwidths (B > 10 kHz) do not really affect the standard deviation in this scenario compared to the rapid decrease around the sweep spot.

Similar to the previous evaluation, the sweep spot in Fig. 14c is located between B = 2 kHz − 5 kHz. In this specific scenario we observe $2/\Delta t_{\text{TOA}}$ = 7.7 kHz. This leads to the assumption that the mentioned sweep spot is located in the area around $B \approx 1/\Delta t_{\text{TOA}}$.

Moreover, in Sect. 5.2 we assumed that a longer symbol length does not notably improve variation. Extending the symbol length by 150 % gives a mean improvement of 5 % in Fig. 14b and 32 % in Fig. 14c for bandwidths higher than $1/\Delta t_{\text{TOA}}$. Thus, the relationship between enhancement of symbol length and the resulting improvement of the standard derivation is comparatively low.

6 GUIDE AND CONCLUSION

Underwater communication is required for the deployment of underwater sensor networks and of swarms of μAUVs, which additionally require a self-localization. One of the major aspects is to find a proper packet synchronization in order to have accurate time-of-flight measurements or a correct data reception. In a shallow-water scenario with LOS conditions, the reflection and scattering at the water surface cause massive interference, because the NLOS signals have low delay and attenuation only.

In summary, our research and real-world evaluations lead to the following instructions to design a chirp-based synchronization in a shallow-water scenario: (1) Discover all of the desired communication distances and water depths. (2) Find the minimum time-of-arrival distance between the LOS path and strongest NLOS path (surface reflection) Δt_{TOA}. (3) Choose a bandwidth $B \geq 1/\Delta t_{\text{TOA}}$. In this region the accuracy gets an intense improvement. However, higher bandwidths also improve the accuracy. The major improvement is in this area. (4) In our cases, the effect of a longer symbol length T is not influential. Shorter symbols enable a faster synchronization. (5) In addition to the symbol parameter, the design of the peak detection algorithm plays a major aspect. The used algorithm has to find the first peak, instead of the highest peak in the cross-correlation function.

We experienced that our finding are also useful in other scenarios. However, in this work we use a high sampling rate and have a powerful computing capacity. The next step is the implementation on our small and low-power underwater modem, without such a high sampling rate and highly limited computing capacity.

ACKNOWLEDGMENT

This work has been partially supported by the German Federal Ministry of Education and Research (BMBF, FKZ 13N14153), the German Federal Ministry for Economic Affairs and Energy (BMWi, FKZ 03SX463C), and ERA-NET Cofund MarTERA (contract 728053).

REFERENCES

[1] M. Alsharef and R. Rao. 2015. M-ary Chirp Modulation for Coherent and non-Coherent Data Transmission. In *Proceeding of the IEEE 28th Canadian Conference on Electrical and Computer Engineering*. Halifax, Canada.

[2] B. Benson, Y. Li, B. Faunce, K. Domond, D. Kimball, C. Schurgers, and R. Kastner. 2010. Design of a Low-Cost Underwater Acoustic Modem. *IEEE Embedded Systems Letters* 2, 3 (Sept 2010), 58–61.

[3] M. S. Caley and A. J. Duncan. 2016. Wide-band Shallow Acoustic Channel Simulation with Realistic Doppler and Delay Spreading for 3D Evolving Rough Surfaces. In *Proc. of the International Conf. Underwater Communications and Networking (UComms)*. Lerici, Italy.

[4] Gianni Cario, Alessandro Casavola, Marco Lupia, and Claudio Rosace. 2015. SeaModem: A Low-Cost Underwater Acoustic Modem for Shallow Water Communication. In *Proc. of the MTS/IEEE Oceans Conf.*

[5] C. E. Cook. 1960. Pulse Compression-Key to More Efficient Radar Transmission. *Proc. of the IRE* 48, 3 (March 1960), 310–316.

[6] Emrecan Demirors and Tommaso Melodia. 2016. Chirp-based LPD/LPI Underwater Acoustic Communications with Code-time-frequency Multidimensional Spreading. In *Proc. of the 11th ACM International Conference on Underwater Networks & Systems (WUWNet '16)*. New York, NY, USA, Article 9, 6 pages.

[7] E. Demirors, G. Sklivanitis, T. Melodia, S. N. Batalama, and D. A. Pados. 2015. Software-defined Underwater Acoustic Networks: Toward a High-Rate Real-Time Reconfigurable Modem. *IEEE Communications Magazine* 53, 11 (Nov. 2015), 64–71.

[8] Evologics GmbH. 2018. Underwater Acoustic Modems. Retrieved September 15, 2018 from http://www.evologics.de/en/products/acoustics/

[9] E. Gallimore, J. Partan, I. Vaughn, S. Singh, J. Shusta, and L. Freitag. 2010. The WHOI Micromodem-2: A Scalable System for Acoustic Communcations and Networking. In *Proc. of the MTS/IEEE Oceans Conf.*

[10] A. Hackbarth, E. Kreuzer, and E. Solowjow. 2015. HippoCampus: A Micro Underwater Vehicle for Swarm Applications. In *Proc. of the IEEE/RSJ International Conf. on Intelligent Robots and Systems (IROS)*. Hamburg, Germany.

[11] John Heidemann, Milica Stojanovic, and Michele Zorzi. 2012. Underwater Sensor Networks: Applications, Advances, and Challenges. *Philosophical Transactions of the Royal Society–A* 370, 1958 (Jan. 2012), 158–175.

[12] Jan Heitmann, Fabian Steinmetz, and Christian Renner. 2018. A Case for Chirp Modulation for Low-Power Acoustic Communication in Shallow Waters. In *Proc. of the 17th GI/ITG KuVS Fachgespräch "Sensornetze"*. Braunschweig, Germany.

[13] Jan Heitmann, Fabian Steinmetz, and Christian Renner. 2018. Self-Localization of Micro AUVs Using a Low-Power, Low-Cost Acoustic Modem. In *Proc. of the OCEANS 2018 (OCEANS)*. Charleston, SC, USA.

[14] Hydromea. 2018. Vertex AUV System Overview. Retrieved September 15, 2018 from http://hydromea.com/vertex_brochure.pdf

[15] T. Jenserud and Sven Ivansson. 2014. Modeling the Power Delay Profile of Underwater Acoustic Channels — The Effects of Out-of-Plane Scattering and Reverberation. In *Proc. of the International Conf. Underwater Communications and Networking (UComms)*. Sestri Levante, Italy.

[16] K. Kebkal, A. Kebkal, R. Bannasch, and S. Yakovlev. 2004. Parameter Estimation of a Sweep-Spread Carrier Signal for Advanced Acoustic Communication via Multipath Shallow Water Channels. In *Proc. of the 7th European Conference on Underwater Acoustics (ECUA)*. Delft, Netherlands.

[17] Konstantin G. Kebkal and Rudolf Bannasch. 2002. Sweep-spread carrier for underwater communication over acoustic channels with strong multipath propagation. *The Journal of the Acoustical Society of America* 112, 5 (2002), 2043–2052.

[18] H. Lee, T. H. Kim, J. W. Choi, and S. Choi. 2015. Chirp signal-based aerial acoustic communication for smart devices. In *2015 IEEE Conference on Computer Communications (INFOCOM)*. 2407–2415.

[19] W. Lei, D. Wang, Y. Xie, B. Chen, X. Hu, and H. Chen. 2012. Implementation of a high reliable chirp underwater acoustic modem. In *2012 Oceans - Yeosu*. 1–5.

[20] Jaime Lloret. 2013. Underwater Sensor Nodes and Networks. *Sensors, Special Issue on Underwater Sensor Nodes and Underwater Sensor Networks* 13, 9 (Sept. 2013), 11782–11796.

[21] X. Lurton. 2010. *An Introduction to Underwater Acoustics*. Springer-Verlag Berlin Heidelberg, Chapter Underwater acoustic wave propagation, 13–74.

[22] MarTERA. 2018. Robotic Vessels as-a-Service. Retrieved September 15, 2018 from https://www.martera.eu/projects/robovaas

[23] David Pinto, Sadraque S. Viana, Jose Augusto M. Nacif, Luiz F. M. Vieira, Marcos A. M. Vieira, Alex B. Vieira, and Antonio O. Fernandes. 2012. HydroNode: A Low Cost, Energy Efficient, Multi Purpose Node for Underwater Sensor Networks. In *Proc. of the 37th IEEE Conf. on Local Computer Networks (LCN)*. Clearwater, FL, USA.

[24] J. Potter, J. Alves, D. Green, G. Zappa, I. Nissen, and K. McCoy. 2014. The JANUS Underwater Communications Standard. In *Proc. of the International Conf. Underwater Communications and Networking (UComms)*. Sestri Levante, Italy.

[25] M. Rao, N. K. Kamila, and K. V. Kumar. 2016. Underwater Wireless Sensor Network for Tracking Ships Approaching Harbor. In *Proc. of the IEEE International Conf. on Signal Processing, Communication, Power and Embedded System (SCOPES)*.

[26] Christian Renner. 2017. Packet-Based Ranging with a Low-Power, Low-Cost Acoustic Modem for Micro AUVs. In *Proc. of the 11th International ITG Conf. on Systems, Communications and Coding (SCC)*. Hamburg, Germany.

[27] Christian Renner and Alexander J. Golkowski. 2016. Acoustic Modem for Micro AUVs: Design and Practical Evaluation. In *Proc. of the 11th ACM International Conf. on Underwater Networks & Systems (WUWNet)*. Shanghai, China.

[28] Francois Sforza. 2013. COMMUNICATIONS SYSTEM. https://patents.google.com/patent/US8406275B2 US Patent No. 8.406.275 B2.

[29] Milica Stojanovic and James Preisig. 2009. Underwater Acoustic Communication Channels: Propagation Models and Statistical Characterization. *IEEE Communications Magazine* (Jan. 2009), 84–89.

[30] FP7 SUNRISE. 2018. SUNRISE FP7 research project. http://fp7-sunrise.eu

[31] G. Toso, P. Casari, and M. Zorzi. 2014. The Effect of Different Attenuation Models on the Performance of Routing in Shallow-Water Networks. In *Proc. of the International Conf. Underwater Communications and Networking (UComms)*. Sestri Levante, Italy.

[32] Tritech International Limited. 2018. Micron Data Modem – Acoustic Modem. Retrieved September 15, 2018 from http://www.tritech.co.uk/product/micron-data-modem

[33] G. Turin. 1960. An introduction to matched filters. *IRE Transactions on Information Theory* 6, 3 (June 1960), 311–329.

[34] James E. Vander Mey and Timothy J. Vander Mey. 1992. SPREAD SPECTRUM COMMUNICATIONS SYSTEM FOR NETWORKS. https://patents.google.com/patent/US5090024A/ US Patent No. 5,090,024.